INL/JOU-23-71237-Revision-0

Pressure Drop Correlation Improvement for the Near-Wall Region of Pebble-Bed Reactors

September 2022

David Reger, Elia Merzari, Yassin Hassan, Haomin Yuan, Yu-Hsiang Lan, Paul Fischer, Misun Min, Paolo Balestra, Sebastian Schunert

Changing the World's Energy Future

INL is a U.S. Department of Energy National Laboratory operated by Battelle Energy Alliance, LLC

INL/JOU-23-71237-Revision-0

Pressure Drop Correlation Improvement for the Near-Wall Region of Pebble-Bed Reactors

David Reger, Elia Merzari, Yassin Hassan, Haomin Yuan, Yu-Hsiang Lan, Paul Fischer, Misun Min, Paolo Balestra, Sebastian Schunert

September 2022

Idaho National Laboratory
Idaho Falls, Idaho 83415

http://www.inl.gov

Prepared for the
U.S. Department of Energy
Under DOE Idaho Operations Office
Contract DE-AC07-05ID14517

Pressure Drop Correlation Improvement for the Near-Wall Region of Pebble-Bed Reactors

David Reger, Elia Merzari

Pennsylvania State University, University Park PA 16803

Paolo Balestra, Sebastian Schunert

Idaho National Laboratory, Idaho Falls, ID 83415

Yassin Hassan

Texas A&M University, College Station TX, 77843

Haomin Yuan, Yu-Hsiang Lan, Paul Fischer, Misun Min

Argonne National Laboratory, Lemont IL, 60439

Abstract

Packed beds play an important role in many engineering fields, with their applications in nuclear energy being driven by the development of next-generation reactors utilizing pebble fuel. The random nature of a packed pebble bed creates a flow field that is complex and difficult to predict. Porous media models are an attractive option for modeling PBRs, as they provide intermediate fidelity results and are computationally efficient. Porous media models, however, rely on the use of correlations to estimate the effect of complicated flow features on the pressure drop and heat transfer in the system. Existing correlations were developed to predict the average behavior of the bed, but they are inaccurate in the near-wall region where the presence of the wall affects the pebble packing. This work aims to investigate the accuracy of a porous media model using the KTA correlation, the most common pressure drop correlation for PBRs, compared to high-fidelity Large Eddy Simulation (LES). A bed of 1,568 pebbles is investigated at Reynolds numbers from 625 to 10,000. The bed is divided into five concentric subdomains to compare the average velocity, friction losses, and form losses between the porous media and LES codes.

The comparison between the LES simulation and the KTA correlation revealed that the KTA correlation largely underpredicts the form losses in the near-wall region, leading to an overprediction of the velocity near the wall by nearly 30%. An investigation of the form losses across the range of Reynolds numbers in the LES results provided additional insight on how the KTA correlation may be improved to better predict these spatial effects in a pebble bed. This data suggests that the form coefficient near the wall must be increased by 48% while decreasing the form coefficient of the inner bulk region of the bed by 15%. The implementation of these improvements to the KTA correlation in a porous media model produced a radial velocity profile that saw significantly improved agreement with the LES results.

Keywords: Pebble Bed Reactor, Pressure Loss, Large Eddy Simulation, Porous Media, Wall-Channel Effect

---

I. Introduction

Recent years have seen increased interest in the development of generation IV nuclear reactors. One of the most mature and proven generation IV reactor types is the pebble bed reactor (PBR), in which the fissile material is contained in microencapsulated particles and embedded into graphite spheres. The graphite spheres are then randomly packed within the reflector blocks to form the reactor core. The coolant, typically either an inert gas or a molten salt, flows through the pebble bed, creating a flow field that is complex in both space and time. As pebble bed reactor designs mature in their development, the need for accurate and efficient calculations for both licensing and design optimization increases. Design basis accidents for PBRs often extend over 10's-100's of hours, making high-fidelity simulations computationally intractable due to the high cost of performing simulation on these time scales. Instead, lower-order methods such as porous media models are the current state of the art. Lower-order models, however, rely on correlations and closures to capture the effects of flow features that are not explicitly modeled. It is therefore imperative to

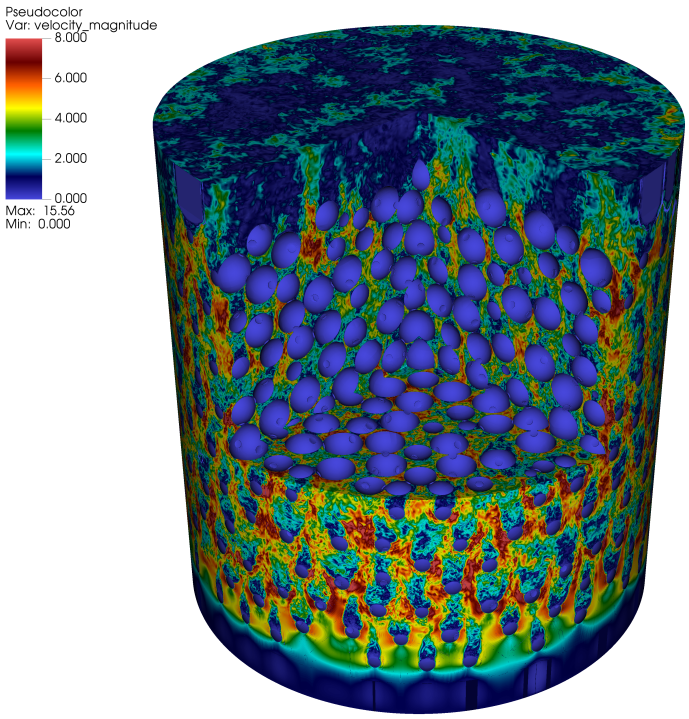

Figure 1: Visualization of the instantaneous velocity magnitude at Re = 3,750 for the 1,568 pebble bed used for this work.

employ correlations that accurately represent the relevant physics of the system.

An area of interest for correlation improvement in these systems is the near-wall region. In the near-wall region, the presence of the wall disrupts the random pebble packing, causing the pebbles to form more orderly structures. Large channels form near the wall, increasing the porosity and creating fast-moving streams of flow. The formation of these fast-moving structures is known as the wall-channeling effect. The flow field in the near-wall region is distinctly different from the flow in the interior of the bed, and thus correlations developed to predict the average pressure drop in the entire bed are not capable of accurately predicting the localized effects near the wall.

Capturing the wall-channeling effect in a packed bed requires an accurate prediction of the pressure drop in each region of the bed. Many previous re-

searchers have worked to develop correlations used to predict the pressure drop in packed beds. The correlation suggested by Ergun [1] using experimental data was one of the first developed for predicting pressure losses in a packed bed. Ergun's correlation expressed the total pressure loss as a sum of viscous friction losses, dominant at low Reynolds numbers, and inertial form losses, dominant at high Reynolds numbers. Mehta and Hawley [2] discovered that Ergun's correlation was inaccurate at low pebble-to-bed diameter aspect ratios due to the larger role that wall effects play in these slender beds. They suggested a correlation that used a difference hydraulic diameter that accounted for the aspect ratio of the bed. This correlation was later improved by Riechelt [3] who performed experimental studies to account for larger ranges of Reynolds numbers, porosities, and aspect ratios. Work by Hicks [4] suggested that the constant friction and form terms used in Erguns equation were not constant, but rather depend on the Reynolds number. In more recent years, Choi [5] developed a model for slender beds that was based on the Ergun equation. In this model, a wall-correction factor is used for the inertial loss term. A sensitivity study was also performed by Wu et. al [6] to investigate the sensitivity of pressure loss to the bed height. Most relevant for this study is the correlation developed by the German Nuclear Safety Standards Commission [7]; this correlation is known as the KTA (Kerntechnischer Ausschuss) correlation. This correlation was developed using experimental data from experiments with conditions similar to those that are found in High-Temperature Gas-Cooled Reactors (HTGRs). For this reason, this correlation has been chosen as the main correlation of comparison for this study and will serve as the basis for improvement.

Numerous studies have also been performed for packed beds that make use of computational methods. A comparison between experimental and simulation pressure drop results was performed by Calis [8] for beds with very low aspect ratios. Atmakadis and Kenig [9] have performed simulations of both regular and irregular packed beds to analyze the wall effects and make comparisons to various correlations. Work by Yildiz [10] performed a Direct Numerical Simulation (DNS) study on a bed of 146 pebbles to compare with available experimental

data and correlations. Additionally, there are currently a number of studies, such as [11] [12] that analyze HTGR designs currently in consideration while using the KTA correlation.

This work intends to further the development of correlations used for HTGRs and FHRs by performing Large Eddy Simulation (LES) of a bed of 1,568 pebbles, pictured in Figure 1. High-fidelity simulation results will be compared to porous media models using the KTA correlation to determine areas of discrepancy. The data will then be used to suggest improvements to the KTA correlation that will allow localized effects to be more accurately modeled.

II. Methods

II.A. NekRS Introduction

The high-fidelity code chosen for this work is Argonne National Laboratory's NekRS spectral-element CFD code [13]. NekRS is an evolution of the well-established open-source Nek5000 code [14], adapted for GPU compatibility. NekRS is capable of linking to Nek5000 to utilize its extensive pre- and post-processing capabilities. NekRS demonstrates excellent scalability, and further details on its performance for nuclear applications can be found in a recent publication [15].

The simulations performed in this work are wall-resolved Large Eddy Simulation (LES) using the incompressible, constant-properties Navier-Stokes equations:

$$\frac{\partial \vec{v_i}}{\partial t} + \vec{v_i} \cdot \nabla \vec{v_i} = -\nabla P + \frac{1}{Re} \nabla^2 \vec{v_i} \tag{1}$$

$$\nabla \cdot \vec{v_i} = 0 \tag{2}$$

Simulations were performed using nondimensional variables according to the following nondimensionalization:

$$x^* = \frac{x}{D_{peb}} \tag{3}$$

$$v^* = \frac{v}{v_{inlet}} \tag{4}$$

$$t^* = \frac{t v_{inlet}}{D_{peb}} \tag{5}$$

$$P^* = \frac{P}{\rho {v_{inlet}}^2} \tag{6}$$

Additionally, a high-pass filter approach was used to mimic the effects of dissipation on the subgrid scales [16]. Simulations were run on the Summit supercomputer using 360 Nvidia V100 GPU's. The cases for the various Reynolds numbers each took roughly 20 hours of simulation time.

II.B. Validation of NekRS

Validation of the Nek5000/NekRS code has previously been performed in a number of existing works. Specifically for pebble beds, work by Yildiz et. al [10] has demonstrated good agreement of first-order statistics between Nek5000 and experimental results. This work also demonstrated that the meshing method of applying chamfers at pebble contact areas does not significantly influence the porosity of the resulting bed. Another work [17] compared velocity profiles in a bed of 67 pebbles between simulation and experiment. Similar agreement to [10] was found. Additional verification and validation studies for Nek5000/NekRS can be found in works by Lai et. al [18] and Obabko et. al [19]

II.C. Mesh Generation

The generation of the pebble bed for this work uses the Discrete Element Method (DEM) implemented in the open-source physics engine Project Chrono [20]. To generate the bed, pebbles were first generated in randomly sampled sheets 2 pebble diameters away from each other. Once these initial sheets were generated, they were dropped down into a cylindrical vessel to pack. The resulting bed had an aspect ratio ($\frac{D_{bed}}{D_{peb}}$) of 13. After the packing was performed, a selection of 1,568 pebble centers were extracted from the middle region of the

resulting bed to avoid packing anomalies that would be found in the bottom and top of the bed.

After the pebble centers have been extracted from the DEM simulation, a meshing script is used to generate an all-hexahedral mesh for use in NekRS. The meshing method for this work was developed as part of the Cardinal multiphysics project [21] and it employs a novel Voronoi-cell approach. First, the script creates a Voronoi cell for the void region around each of the pebbles. After the Voronoi cells are created, a number of processing steps such as edge collapse, vertex insertion, and facet tessellation are performed to generate an all-hexahedral mesh. This meshing method assumes that all pebbles are perfectly spherical. At points of pebble contact, a small chamfer is added to remove singular mesh points. More details on the generation of the mesh may be found in a recent publication [**?**]. The mesh resolution of the resulting mesh is designed to resolve Taylor micro-scales within the domain based on estimates from a previous work [10]. The boundary layer is well-resolved with at least one point below $y^+ < 1$ and at least five points with $y^+ < 10$. An inlet boundary condition with a flat profile is applied along with a stabilized outflow condition at the outlet [22]. Additionally, a no-slip boundary condition is applied at the pebble and cylinder wall boundaries.

The radial porosity distribution is a critical part of this work, as the radial porosity distribution will largely govern the distribution of flow to different regions of the bed. The radial porosity profile was calculated in NekRS by separating the domain into $0.05D_{peb}$ wide concentric cylinders and calculating the fluid volume in each. This was done in NekRS by summing the volume of all fluid elements that fell within each region. The porosity is the ratio of the fluid volume to the total volume of the annulus. This calculation was performed over the entire axial height of the bed, excluding the inlet and outlet regions and 2 layers of pebbles on the top and bottom of the bed. This porosity profile was then compared in Figure 2 to the theoretical radial porosity profile correlation proposed by de Klerk [23].

The radial porosity profile that resulted from the NekRS case shows very

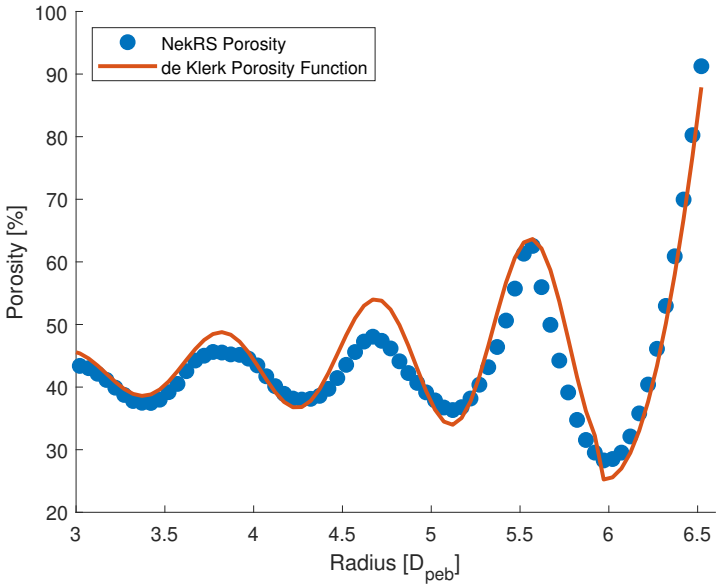

Figure 2: Radial porosity profile seen in the NekRS mesh and predicted by the de Klerk porosity correlation.

good agreement with de Klerk's correlation in the near-wall region. Throughout the entire bed, the shape of the porosity function matches very well between the DEM bed and the de Klerk correlation. There is some discrepancy, however, in the magnitude of these porosity variations that are seen towards the interior of the bed, where the simulation case had a porosity slightly below the de Klerk value. It should be noted, however, that the accuracy of the de Klerk correlation is sensitive to the value of ϵ_b that is used which could potentially be causing this discrepancy.

II.D. Pronghorn Introduction

Idaho National Laboratory's (INL) Pronghorn code [24] was used as the intermediate-fidelity code for this work. Pronghorn is a coarse-mesh finite element thermal hydraulics code built on the Multiphysics Object-Oriented Simulation Environment (MOOSE) framework [25]. The use of the MOOSE framework allows Pronghorn to be easily coupled with other MOOSE codes to perform mul-

tiphysics analysis. Pronghorn is intended to provide results for steady-state and transient simulations with short execution times to provide boundary conditions for system-level analysis and carry out design-scoping studies. Pronghorn is capable of using a variety of solver models, but the incompressible porous-media Navier Stokes equations were used for this study:

$$\epsilon \frac{\partial \rho_f}{\partial t} + \nabla \cdot (\epsilon \rho_f \vec{v_i}) = 0, \tag{7}$$

$$\epsilon \frac{\partial (\rho_f \vec{v_i})}{\partial t} + \nabla \cdot (\epsilon \rho_f \vec{v_i} \vec{v_i}) + \epsilon \nabla P - \epsilon \rho_f \vec{g} + W \rho_f \vec{v_i} - \nabla \cdot (\mu \nabla \vec{v_i}) = 0, \tag{8}$$

II.E. Correlation Used

The main drag correlation of interest for this study is the KTA correlation, developed by the German Nuclear Safety Standards Commission in 1981 [7]. This correlation was developed using experimental data for conditions that are specifically applicable to HTGRs. The KTA correlation is valid for $0.36 < \epsilon < 0.42$ and $10 < Re_m < 100,000$. The KTA correlation is as follows:

$$\frac{\Delta P}{L} = \left(\frac{320}{Re_m} + \frac{6}{{Re_m}^{0.1}} \right) \left(\frac{1-\epsilon}{\epsilon^3} \right) \left(\frac{\rho^2 {v_s}^2}{D_p} \right) \left(\frac{1}{2\rho} \right) \tag{9}$$

where the $\frac{320}{Re_m}$ term represents the viscous frictional losses and the $\frac{6}{Re_m^{0.1}}$ term represents the inertial form losses. The KTA correlation is developed to represent the average pressure drop of the entire bed, and does not explicitly model any wall-channeling effects.

II.F. Comparison Methodology

A critical aspect of this work is the method of comparison between the high-fidelity and intermediate-fidelity results. Given the much more complex representation of the system in the high-fidelity model, multiple simplifications were required to produce results that could be compared with the porous media model. This was achieved by separating the system into multiple concentric subdomains and extracting spatial averages for each of these rings. For this

Table I: Geometry of the five concentric subdomains used for postprocessing.

Ring	Inner Radius	Outer Radius	Average Porosity
1	0.0	5.575	0.43687
2	5.575	5.825	0.43804
3	5.825	6.075	0.30147
4	6.075	6.325	0.43531
5	6.325	6.575	0.67357

work, a ring width of 0.25 pebble diameters was chosen. This ring width provides enough resolution to capture the effect of velocity channeling near the wall in a single ring. As a result of the porosity profile in Figure 2, the radial velocity profile takes a similar shape. Given that the oscillatory motions have a period of roughly 1 pebble diameter, the effect of channeling near the wall will be seen for roughly 1/4 of a pebble diameter away from the wall. This can be seen in Figure 2, where the porosity is significantly higher than the bulk value from the edge of the wall to 1/4 of a pebble diameter in from the wall where it then will dip below the bulk porosity as it continues the oscillation inwards. The rings were axially centered on the bed and spanned the entire height of the bed except for 2 pebble diameters at the top and bottom of the bed to avoid entrance and exit effects. The average fluid velocity, pressure gradient, wall shear, and porosity were calculated for each ring. The porous media code could then model each of these rings with their respective porosity calculated from the high-fidelity geometry to create an equivalent system. Averages for each ring were extracted directly from the porous media code and compared to the LES data. Geometric information and the average porosity for the five rings can be found in Table I along with an example of the two models in Figure 3.

Another challenge is the separation of friction and form losses in the high-fidelity data. A key element of this work is the formation of the methodology to extract these parameters. First, the pressure gradient as a result of frictional losses is computed from the definition in the KTA equation:

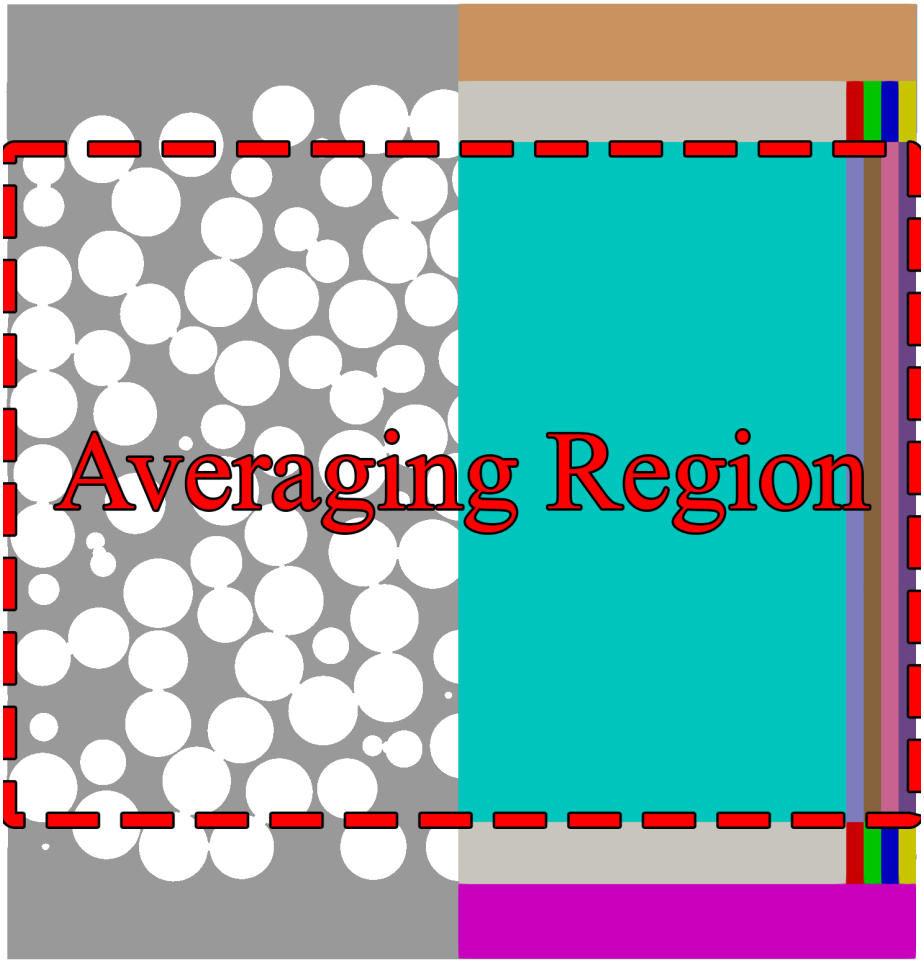

Figure 3: Centerplane slice of the NekRS case (left) and slice of the Pronghorn case with the mesh blocks visible (right). The axial averaging region is shown in the dotted red box.

$$\frac{\Delta P}{L}_{friction} = \left(\frac{320}{Re_m}\right)\left(\frac{1-\epsilon}{\epsilon^3}\right)\left(\frac{\rho^2 {v_s}^2}{D_p}\right)\left(\frac{1}{2\rho}\right) \tag{10}$$

The pressure gradient from form losses was then calculated by subtracting the frictional gradient from the total pressure gradient:

$$\frac{\Delta P}{L}_{form} = \frac{\Delta P}{L}_{total} - \frac{\Delta P}{L}_{friction} \tag{11}$$

Finally, the form coefficient was determined from the form pressure gradient.

$$C_{form} = \frac{2\frac{\Delta P}{L}_{form}}{\rho {v_s}^2} \tag{12}$$

It should be noted that this approach assumes that the friction losses are correctly predicted by the KTA equation for any region of the bed. This assumption is justified, as the friction losses will account for $< 10\%$ of the total losses in the Reynolds number used for this study, meaning that errors with the KTA frictional loss term will not significantly influence the results. We assert that this methodology and the suggested improvements that result from it may not be accurate for $Re_m < 100$ where frictional losses contribute more significantly.

III. Results

III.A. Convergence of Results

A convergence study was performed on the results to ensure that time convergence and mesh convergence were achieved. Time convergence of the Pronghorn results were performed with MOOSE's built-in steady-state detection, where the simulation was run until the relative residual changes by less than 1e-8 between timesteps. The NekRS simulations were all run for roughly 10 convective units (1 convective unit $\rightarrow t^* = 1$) before averaging began. After this initialization, averaging began and the simulation was run for an additional 10 convective units to investigate the convergence of the near-wall velocity. Table II shows the results of this time convergence study. Even the smallest averaging period

Table II: Time convergence of the near-wall velocity average from NekRS

# Convective Units	Average Near-Wall Ring Velocity
2.5	2.963
5	2.965
10	2.966

Table III: Mesh convergence of the near-wall velocity average from NekRS

Polynomial Order	Average Near-Wall Ring Velocity
5	2.964
7	2.965
9	2.965

of 2.5 convective units appears to be sufficient to have a converged near-wall ring average velocity. A mesh convergence study was also performed by changing the polynomial order in the NekRS simulation. Table III shows that the mesh resolution is sufficient to converge the near-wall velocity magnitude, and a polynomial order of 7 was used to generate further results.

III.B. Velocity profiles comparison

The initial comparison between the two codes investigates the predicted velocity profiles in order to quantify the discrepancy between them. Comparisons were done at Reynolds numbers of 2,500, 5,000, and 10,000 to gauge if the velocity and drag profiles displayed a dependency on the Reynolds number. The radial velocity profiles for the three Reynolds numbers are pictured in Figure 4.

The velocity profiles do not display a strong dependency on the Reynolds number, with the near-wall region having an average streamwise velocity of roughly 2.9 across all three Reynolds numbers. Additionally, the KTA correlation overestimates the velocity in the near-wall region by more than 30%. It is thus concluded that an accurate representation of the porosity in a porous media model does *not* lead to an accurate prediction of the velocity near the wall. Rather, it is necessary to modify the pressure drop correlation near the wall to

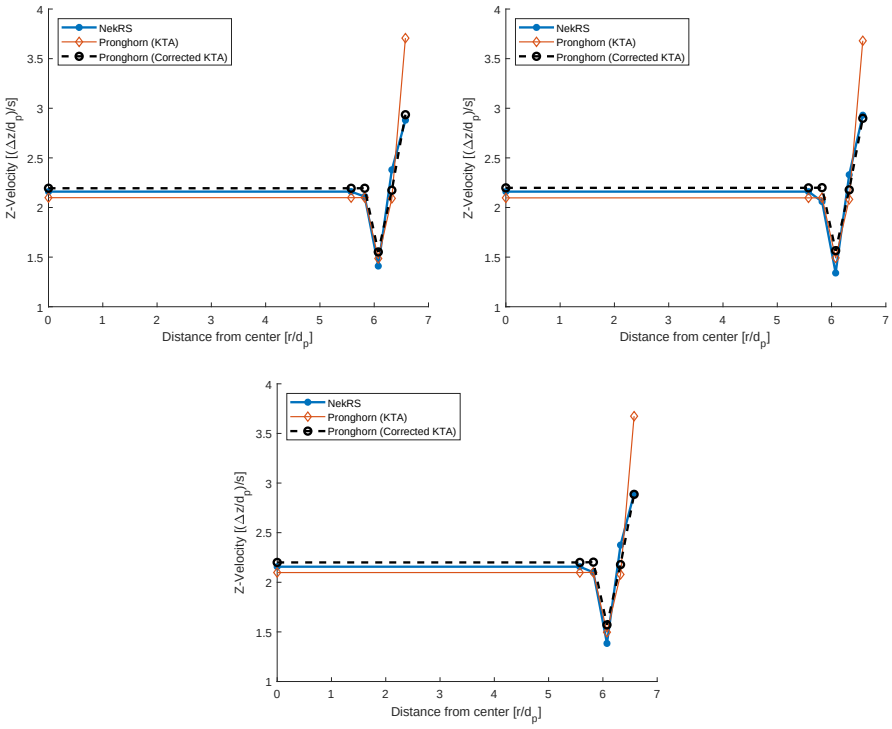

Figure 4: Radial velocity profiles for the NekRS, Pronghorn KTA, and Pronghorn with manual adjustments cases

account for the difference in flow patterns to obtain accurate velocity profiles. Once the discrepancy between the KTA correlation and the LES simulation was established, the form coefficient in the near-wall ring was manually increased in Pronghorn until the velocity in this ring matched the NekRS result. The purpose of this exercise was twofold: firstly, it would serve to demonstrate that the alteration of the form coefficient in the near-wall region would be sufficient to improve the overall velocity profile; secondly, this exercise would verify the process for extracting friction and form coefficients from NekRS and allow the form and friction data to be extracted directly from the LES results rather than manually guess-and-checking in Pronghorn.

III.C. Friction Factor Comparison

The friction factors calculated in each ring from the NekRS and Pronghorn simulations can be found in Figure 5. From these plots, it can be seen that the KTA correlation tended to overpredict the friction factor compared to NekRS in all rings except for the outer ring. It is worth noting that the pressure drop from friction was small in this case compared to the form losses, with the form losses ranging from 85% to 95% of the total losses in each of the rings. As a result, the friction factor was not modified for this study. When the form factor was manually altered, the friction factor saw a slight change due to the slightly different velocity in each of the rings. The friction factors normalized to the value in the first ring are also included in Figure 6. As expected, the rings with porosity that is farthest outside of the valid KTA range see the largest discrepancy between NekRS and the KTA correlation. The shape of these plots remained consistent across the three Reynolds numbers, indicating that the Reynolds number will not have a large effect on the radial distribution of the friction losses in the bed. Once again, this is not of great importance to this study where the role of friction is minor, but may be important for future studies at low Reynolds number.

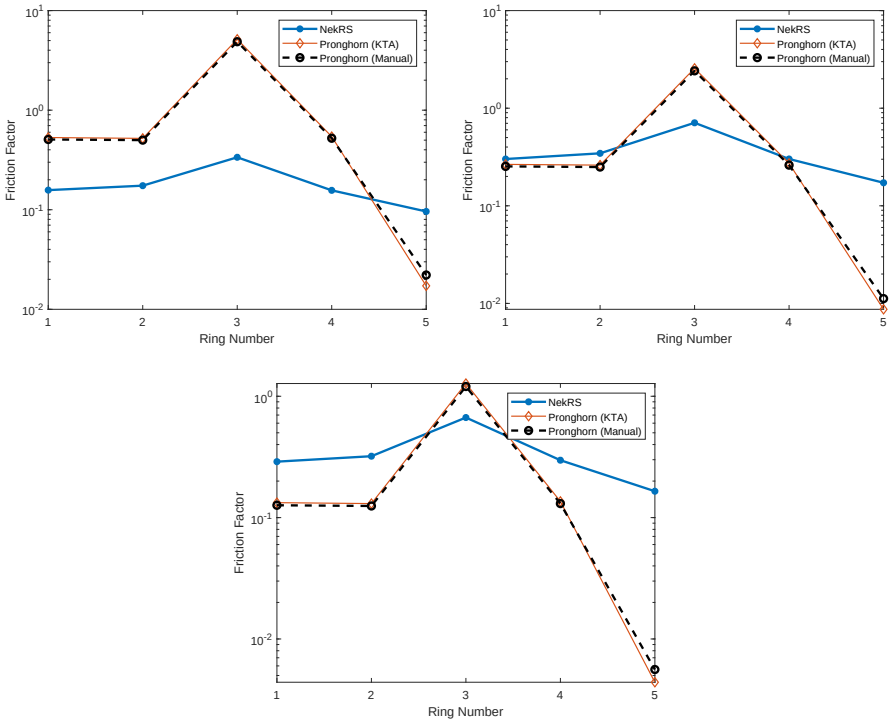

Figure 5: Friction factor in each ring for the NekRS, Pronghorn, and Manually-adjusted Pronghorn cases for Reynolds numbers of 2,500 (left), 5,000 (center), and 10,000 (right)

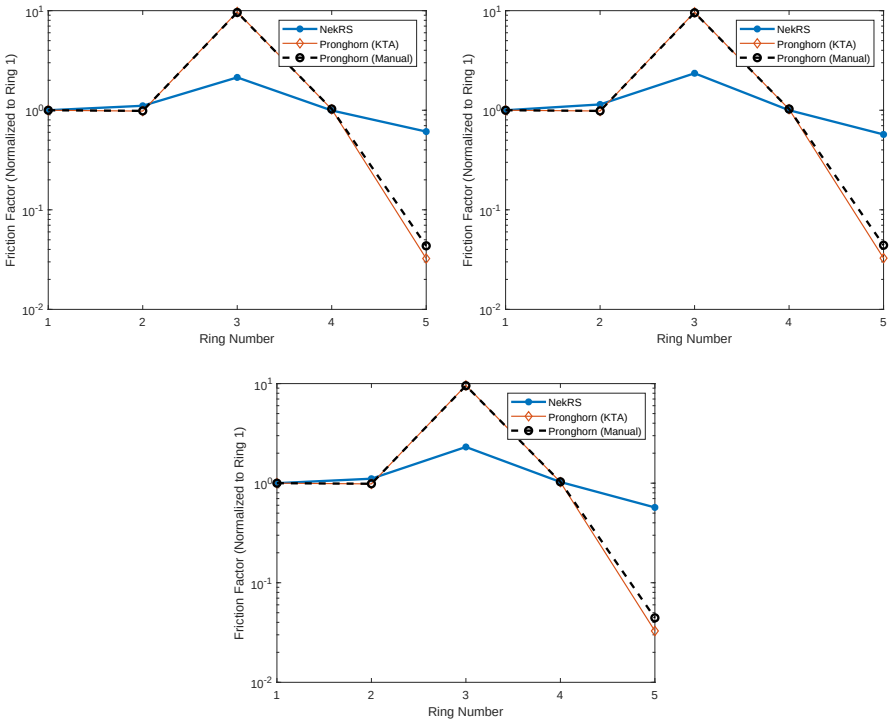

Figure 6: Friction factor in each ring normalized by the first ring for the NekRS, Pronghorn, and Manually-adjusted Pronghorn cases for Reynolds numbers of 2,500 (left), 5,000 (center), and 10,000 (right)

III.D. Form Factor Comparison

Figure 7 shows a comparison of the form factors calculated from the NekRS and Pronghorn results. Similarly to the friction factor results, the KTA correlation tended to overpredict the form factor in all but the outermost ring. After increasing the coefficient in ring five to match the velocity seen in the NekRS results, the form coefficient in the outermost ring was larger than the NekRS coefficient as well. A better understanding of why the velocity profile matches even with this overestimation can be gained by examining the normalized form factors in Figure 8. It can be seen from these plots that the increase in the form factor in the near-wall ring caused the ratio of form factors in each ring to match more closely with what was seen in the NekRS results. This result aligns with intuition and serves to verify that the process of extracting these form coefficients is appropriate. One would expect that the magnitude of the average form coefficient determines the pressure drop and that the ratio between the form coefficients in each ring should determine how much flow each receives.

III.E. Pressure Drop Comparison

In addition to the friction and form factors, a comparison of the pressure gradients between the NekRS and KTA results was also performed and can be found in Figure 9. The KTA values were extracted from the 5-ring Pronghorn model. As expected given the lower form coefficients seen in the NekRS simulation, the pressure drop as well is lower than what is predicted by the KTA correlation. It should be noted, however, that the pressure drop calculated by NekRS was within the quoted range of error given for the KTA correlation.

III.F. Near-Wall Region Correlation Improvements

After verifying the methodology of extracting the friction and form coefficients from the high-fidelity data, it was possible to perform an examination into the trend of the near-wall form coefficients across a large range of Reynolds numbers. The average form coefficient was calculated in ring five for Reynolds numbers ranging from 625 to 10,000. A plot of the form coefficient versus the

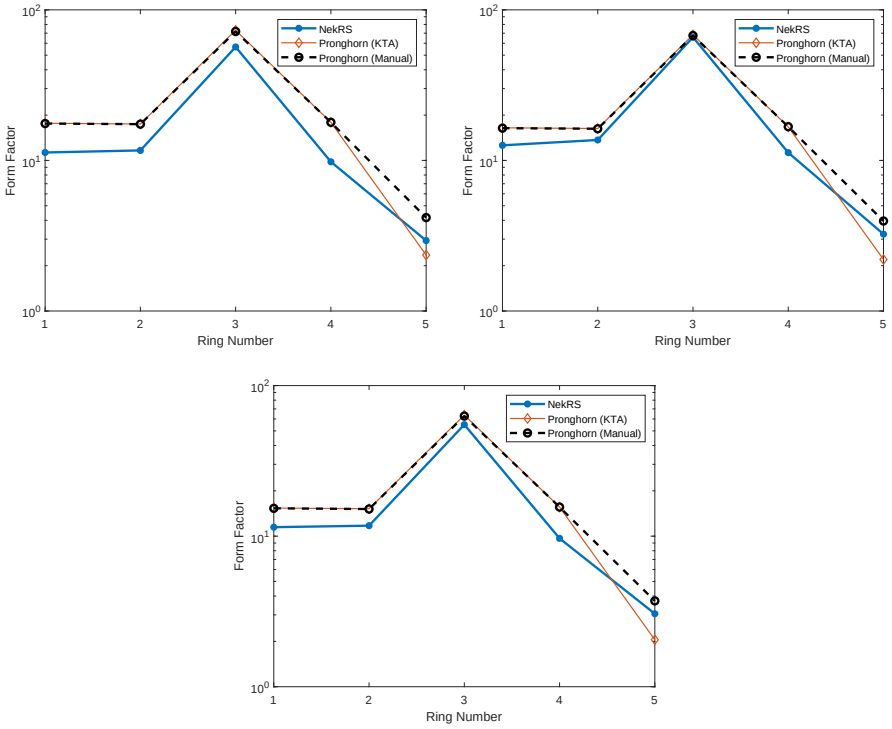

Figure 7: Form factor in each ring for the NekRS, Pronghorn, and Manually-adjusted Pronghorn cases for Reynolds numbers of 2,500 (left), 5,000 (center), and 10,000 (right)

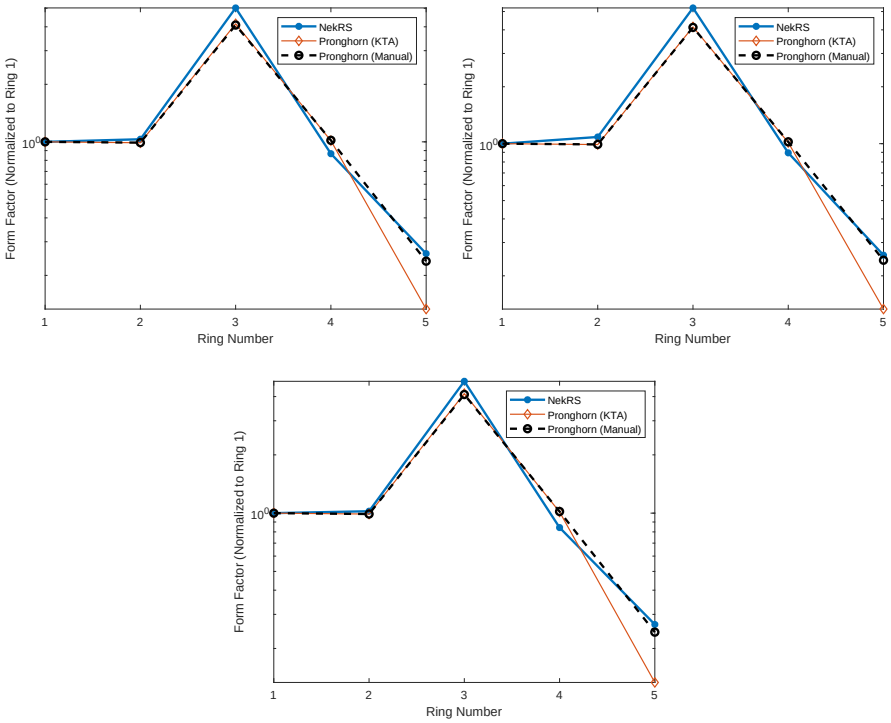

Figure 8: Form factor in each ring normalized by the first ring for the NekRS, Pronghorn, and Manually-adjusted Pronghorn cases for Reynolds numbers of 2,500 (left), 5,000 (center), and 10,000 (right)

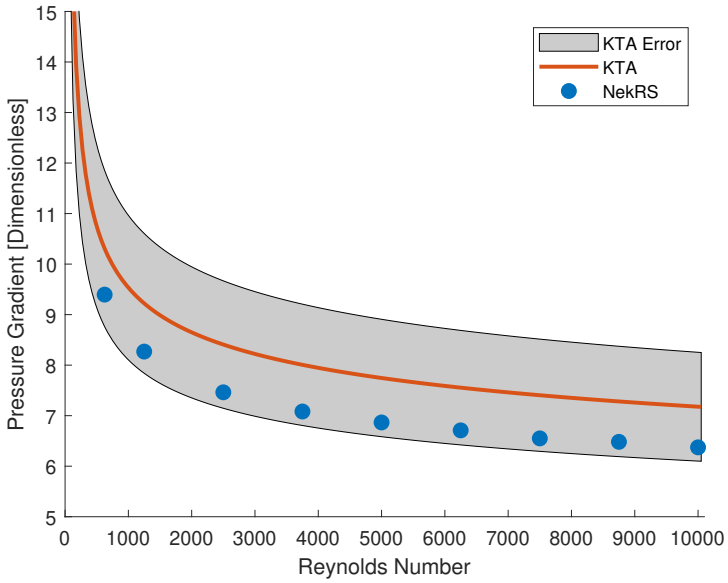

Figure 9: Dimensionless pressure gradient (P^*/x^*) predicted by NekRS and the KTA correlation for Reynolds numbers from 625 to 10,000.

modified Reynolds number in the ring can be found in Figure 10. As expected from the verification exercise, the KTA correlation tended to underpredict the form coefficient near the wall. The dependency of the form coefficient on the modified Reynolds number, however, did match well with what was predicted by the KTA correlation. From this information, we can suggest an increase of the KTA form coefficient in the near-wall region as follows:

$$C_{form} = \frac{6}{Re_m^{0.1}} \rightarrow \frac{8.9}{Re_m^{0.1}} \tag{13}$$

III.G. Bulk Ring Correlation Improvements

The form coefficient in the inner bulk ring was also investigated to determine if it too would see discrepancy compared to the NekRS results. As was done with the near-wall ring, the form coefficient was calculated in ring one for Reynolds numbers from 625 to 10,000. The plot of these form coefficients versus the modified Reynolds number is pictured in Figure 11. It can be seen from this

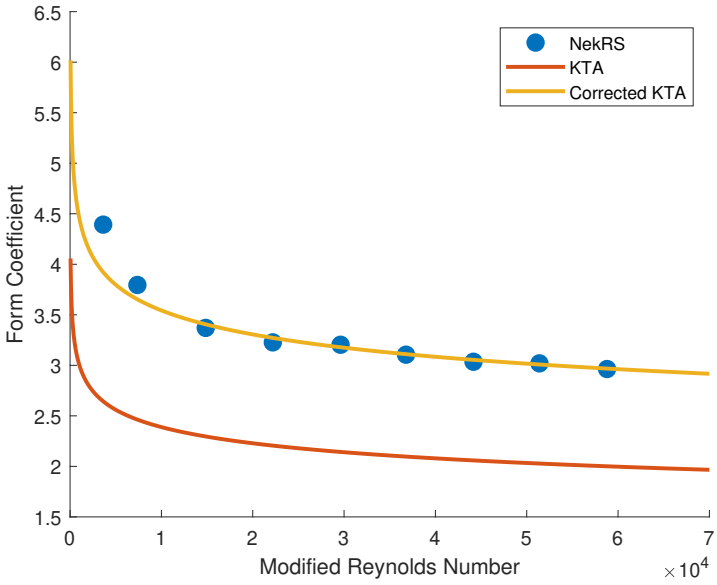

Figure 10: Form coefficient in the near-wall ring (Ring 5) for Reynolds numbers from 625 to 10,000. The value predicted by the KTA correlation is shown along with the NekRS data and it's curve fit.

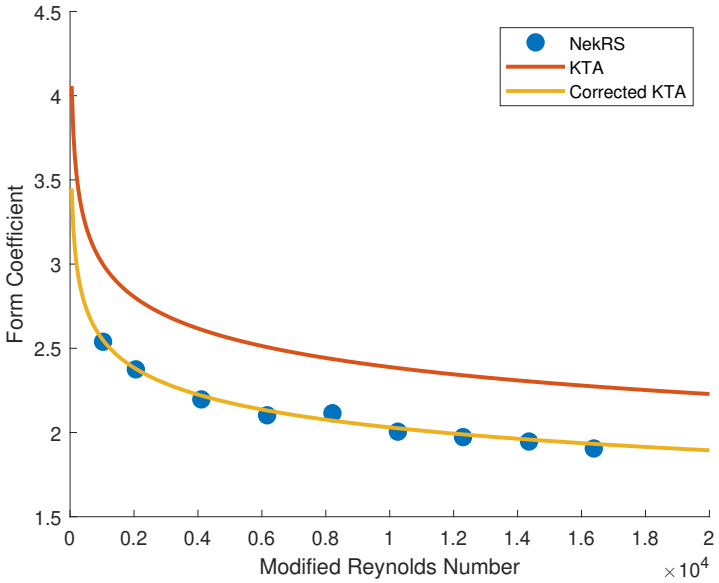

Figure 11: Form coefficient in the bulk ring (Ring 1) for Reynolds numbers from 625 to 10,000. The value predicted by the KTA correlation is shown along with the NekRS data and it's curve fit.

plot that the KTA correlation tends to overpredict the form coefficients in the bulk of the bed. This data suggests the following modification to the KTA form coefficient in the bulk region of the bed:

$$C_{form} = \frac{6}{Re_m^{0.1}} \rightarrow \frac{5.1}{Re_m^{0.1}} \tag{14}$$

III.H. Implementation in Pronghorn

The suggested improvements from the above sections were implemented for the bulk and near-wall rings in the Pronghorn model. The resulting radial velocity profile can be found in Figure 12. The suggested improvements provide substantial improvement over the KTA correlation in the prediction of the near-wall velocity. It is worth noting that making the suggested changes in rings 1 and 5 worsens the velocity agreement in the unchanged rings. If the radial

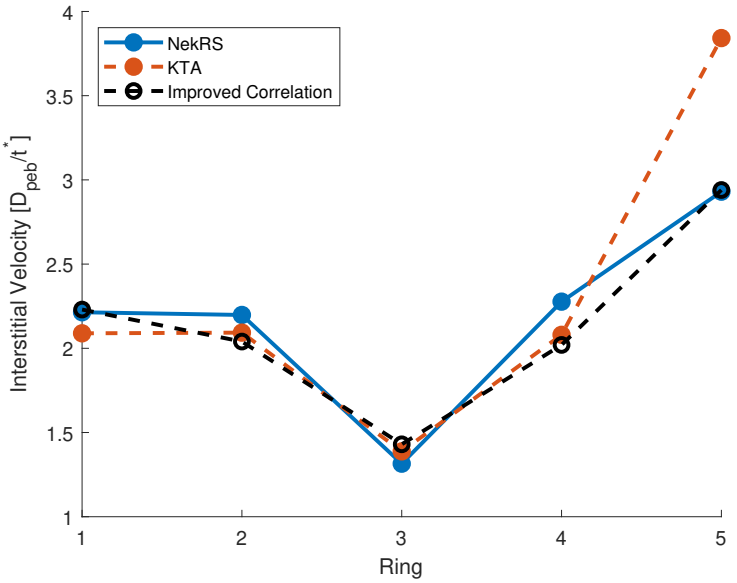

Figure 12: Velocity in each ring the 1,568 pebble bed from NekRS, the KTA correlation, and the suggested improved correlations of this work

velocity profile is to be generally matched better, all rings would need to have improvements applied to them.

III.III.H.1. Preliminary Verification

The results presented thus far have been extracted from only a single bed of 1,568 pebbles. It is important, however, to verify that the improvements suggested based on these results hold consistent for other beds. To test that this is the case, a second bed of roughly 1,700 pebbles was simulated using NekRS, and the same postprocessing procedure was once again performed. An equivalent model was built in Pronghorn for this bed of 1,700 pebbles, and the case was simulated with the KTA correlation. The porous media simulation was then performed using the suggested improvements from this work. The results of these simulations can be seen compared to the NekRS result in Figure 13.

The agreement between the improved correlation and the NekRS result is not quite as good with this bed compared to the 1,568 pebble bed that was

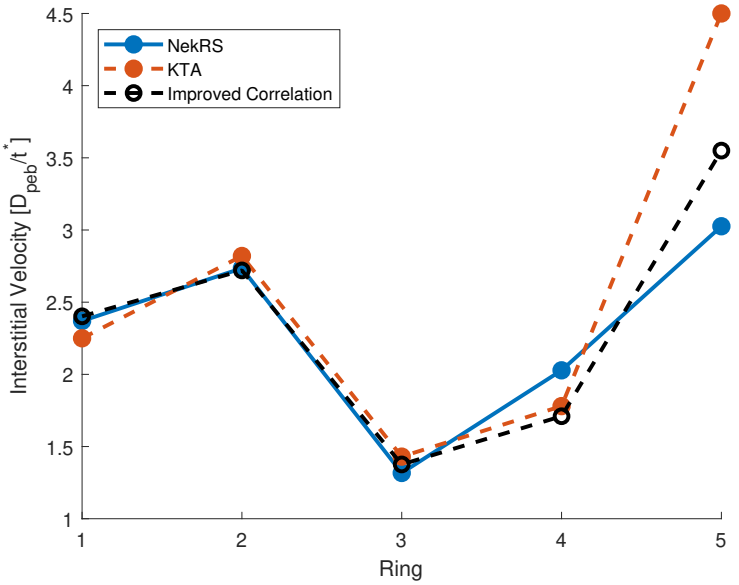

Figure 13: Velocity in each ring for a bed of 1,700 pebbles from NekRS, the KTA correlation, and the suggested improved correlations of this work

used to generate the correlation improvements. Regardless, the improvements still manage to produce a velocity profile that agrees more with the NekRS results than the KTA correlation. Additional work will continue to verify that the suggested correlations produce improved results for beds of different sizes, aspect ratios, and Reynolds numbers.

III.I. Discussion on Ring Size

It should be noted that the choice of ring size to discretize the near-wall region is somewhat arbitrary. A user of a porous-media code may see a need to resolve more or less of the near-wall region depending on their application. We note, however, that the methodology described in this work can be used for any number or size of ring. For instance, if a user desires to use two outer rings of width $0.5D_{peb}$, the same process may be used to extract the form coefficients, determine a new form-term constant for the near-wall ring, and achieve similar improvement over the KTA equation. We note that in this configuration, Ring

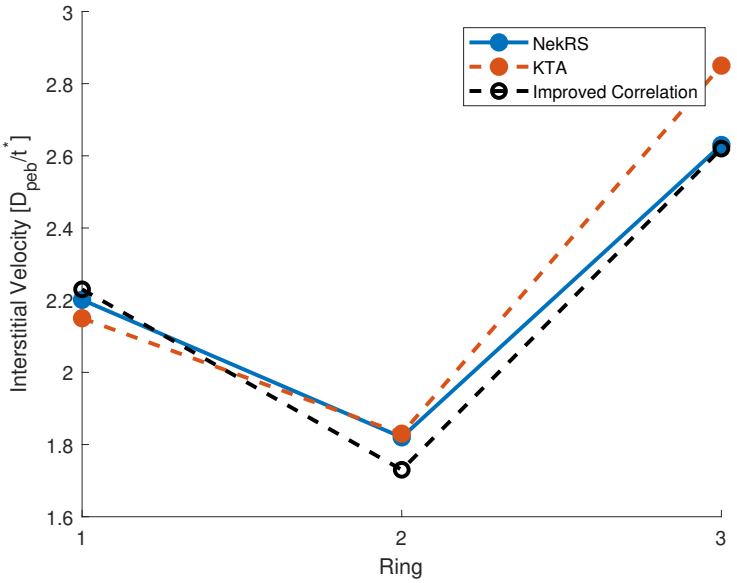

Figure 14: Velocity in each ring for a three-ring model of the 1,568 pebble bed from NekRS, the KTA correlation, and the suggested improved correlations of this work

1 (the inner ring) would remain unchanged from the previous 5-ring model. The overall improvement is demonstrated in Figure 14, where it was determined that for this configuration, the near-wall form coefficient should follow:

$$C_{form} = \frac{6}{Re_m^{0.1}} \rightarrow \frac{6.5}{Re_m^{0.1}} \tag{15}$$

Again, since the inner ring is unchanged, we use the same improvement suggested in Equation 14 for that ring. We recognize that determining a new correlation every time the discretization is changed is not practical. Future work will use the methodology described in this work to determine a generalized improved correlation that will be valid for any given discretization.

IV. Conclusion

This work presented an investigation into the friction and form losses seen in a packed bed. A bed of 1,568 pebbles was packed with DEM simulation and

used to create the high-fidelity mesh. The spectral-element CFD code NekRS was used to produce high-fidelity simulation results, and the Pronghorn porous-media code was used to generate comparative intermediate-fidelity results using the KTA correlation. Postprocessing was necessary to make comparisons between the NekRS and Pronghorn results possible. This was performed by separating the domain into five concentric cylinders. Starting from the wall, 4 cylinders of width 0.25 D_{pebble} were created to provide adequate resolution in the near-wall region. The other ring captured the rest of the bed to represent the bulk bed behavior. Porosity averages were extracted from each of these rings to be used as inputs to the porous-media code to create an equivalent model. Other variables such as the average fluid velocity and pressure drop were also extracted. The frictional pressure drop was first determined using the KTA equation. Then, the frictional pressure drop could be subtracted from the total pressure drop, yielding the form pressure drop. This form pressure drop could then be used to calculate the form coefficient.

Comparison of the radial velocity profile between the NekRS and Pronghorn results at Reynolds numbers of 2,500, 5,000, and 10,000 displayed a significant overprediction of the velocity near the wall when using the KTA correlation in Pronghorn. To verify that the methodology of extracting drag coefficients was appropriate, a verification case was investigated in which the form coefficient in the near-wall ring was manually increased in the Pronghorn model until the velocity in this ring matched the NekRS result. After this change, the form and friction coefficients were analyzed from the NekRS, KTA, and manual adjustment cases. It was found that the KTA correlation tended to overpredict the friction and form coefficients compared to the NekRS simulation in all rings except for the near-wall ring. The manual increase of the form coefficient to get the velocity near the wall to match revealed that in this case, the ratio between the form coefficients in the bulk and near-wall rings matched closely with the NekRS result. This finding served to verify that the method of extracting the form coefficient was appropriate, and the form coefficient for all five rings was then extracted at several additional Reynolds numbers ranging from 625 to

10,000.

By plotting the form coefficient in each ring against the modified Reynolds number, it became evident that the KTA correlation significantly underpredicted the form losses in the near-wall region. The trend of the form coefficient with respect to the modified Reynolds number, however, was consistent between the NekRS data and the KTA correlation. Therefore, it is suggested that within $0.25D_{peb}$ of the wall, the constant in the form term of the KTA is increased from 6 to 8.9.

The most important factor to determining the amount of flow the near-wall region receives is the ratio between the near-wall form loss and the bulk-region form loss. As a result, the same approach used to improve the near-wall ring was applied to the bulk ring, and it is suggested that the constant in the KTA form term is decreased from 6 to 5.1.

The use of these suggested correlations for the near-wall and bulk rings in Pronghorn displayed significantly improved agreement with the NekRS result compared to the KTA equation. A second bed of 1,700 pebbles was also simulated in NekRS and Pronghorn to provide a second case for comparison. Improvement over the KTA correlation was seen when using the suggested improvements, although the agreement was not as good as what was seen in the 1,568 pebbles case.

Future work will seek to further expand on the methodology discussed in this work to develop a more generalized correlation for the form losses. This may be accomplished by gathering additional data for other beds of different sizes to check for inaccuracies with the suggested improvements. Additionally, future simulations will add heating to the pebbles to compare with existing heat transfer correlations to identify gaps in predictive heat transfer capabilities.

Nomenclature

CFD Computational Fluid Dynamics

DEM Discrete Element Method

DNS Direct Numerical Simulation

DOE Department of Energy

FHR Flouride-Cooled High-Temperature Reactor

GPU Graphics Processing Unit

HTGR High-Temperature Gas-Cooled Reactor

LES Large Eddy Simulation

MOOSE Multiphysics Object-Oriented Simulation Environment

PBR Pebble Bed Reactor

ϵ Porosity

ρ Density

τ_w Wall Shear Stress

C_{form} Forccheimer Form Factor

D_h Hydraulic Diameter

D_{peb} Pebble Diameter

f Darcy Friction Factor

g Gravitational acceleration constant

P Pressure

Re Reynolds Number ($\frac{\rho v_s D_{peb}}{\mu}$)

Re_m Modified Reynolds Number ($\frac{Re}{1-\epsilon}$)

t Time

v_i Interstitial Velocity

v_s Superficial Velocity

References

[1] S. Ergun, Fluid flow through packed columns, Journal of Chemical Engineering Progress 48 (2) (1952) 89–94.

[2] D. Mehta, M. Hawley, Wall effect in packed columns, Industrial & Engineering Chemistry Process Design and Development 8 (2) (1969) 280–282.

[3] W. Reichelt, Zur berechnung des druckverlustes einphasig durch- stromter kugel- und zylinderschuttungen, Rheological Acta 17 (1978) 676–692.

[4] R. Hicks, Pressure drop in packed beds of spheres, Industrial & Engineering Chemistry Fundamentals 9 (3) (1970) 500–502.

[5] Y. Choi, S. Kim, D. Kim, A semi-empirical correlation for pressure drop in packed beds of spherical particles, Transport in Porous Media 75 (2) (2008) 133–149.

[6] J. Wu, B. Yu, M. Yun, A resistance model for flow through porous media, Transport in Porous Media 71 (3) (2008) 331–343.

[7] K. Ausschusses, KTA, Reactor core design of high-temperature gas-cooled reactors - part 3: Loss pressure through friction pebble bed cores.

[8] H. P. A. Calis, J. Nijenhuis, B. C. Paikert, F. M. Dautzenberg, C. M. van den Beek, Cfd modelling and experimental validation of pressure drop and flow profile in a novel structured catalytic reactor packing, Chemical Engineering Science 56 (2001) 1713–1720.

[9] E. Kenig, T. Atmakidis, Cfd-based analysis of the wall effect on the pressure drop in packed beds with oderate tube/particle diameter ratios in the laminar flow regime, Chemical Engineering Journal 155 (1-2) (2009) 404–410.

[10] M. A. Yildiz, G. Botha, H. Yuan, E. Merzari, R. Kurwitz, Y. A. Hassan, Direct numerical simulation of the flow through a randomly packed pebble bed, Journal of Fluids Engineering 142 (4).

[11] S. Jun, Z. Yanhua, L. Fu, Various bypass flow paths and bypass flow ratios in htr-pm, Energy Procedia 39 (2013) 258–266.

[12] D. Reger, E. Merzari, P. Balestra, R. Stewart, Improved point kinetic parameters generation for pebble bed reactor transient simulation using neams tools, in: Transactions of the American Nuclear Society, 2021.

[13] P. Fischer, S. Kerkemeier, M. Min, Y. H. Lan, M. Phillips, T. Rathnayake, E. Merzari, A. Tomboulides, A. Karakus, N. Chalmers, T. Warburton, Nekrs, a gpu-accelerated spectral element navier-stokes solver.

[14] P. Fischer, J. Lottes, S. Kerkemeier, O. Marin, K. Heisey, E. Obabko, E. Merzari, Y. Peet, Nek5000 user documentation, Argonne National Laboratory, Lemont, IL, Report No. ANL/MCS-TM-351.

[15] E. Merzari, P. Fischer, M. Min, S. Kerkemeier, A. Obabko, D. Shaver, H. Yuan, Y. Yu, J. Martinez, L. Brockmeyer, et al., Toward exascale: overview of large eddy simulations and direct numerical simulations of nuclear reactor flows with the spectral element method in nek5000, Nuclear Technology 206 (9) (2020) 1308–1324.

[16] S. Rezaeiravesh, R. Vinuesa, P. Schlatter, On numerical uncertainties in scale-resolving simulations of canonical wall turbulence, Computers & Fluids (2021) 105024.

[17] D. Reger, E. Merzari, H. Yuan, S. King, Y. Hassan, K. Ngo, P. Balestra, S. Schunert, Large eddy simulation of a 67-pebble bed experiment, in: Advances in Thermal-Hydraulics, 2022.

[18] J. Lai, E. Merzari, Y. Hassan, P. Fischer, O. Marin, Verification and validation of large eddy simulation with nek5000 for cold leg mixing benchmark, Nuclear Engineering and Design 358.

[19] A. Obabko, P. Fischer, O. Marin, E. Merzari, D. Pointer, Verification and validation of nek5000 for t-junction, matis, siberia, and max experiments., in: Internation Conference on Nuclear Reactor Thermal Hydrualics, 2015.

[20] Project Chrono Development Team, Chrono: An Open Source Framework for the Physics-Based Simulation of Dynamic Systems, https://github.com/projectchrono/chrono.

[21] E. Merzari, H. Yuan, M. Min, D. Shaver, R. Rahaman, P. Shriwise, P. Romano, A. Talamo, Y. Lan, D. Gaston, R. Martineau, P. Fischer, Y. A. Hassan, Cardinal: A lower length-scale multiphysics simulator for pebble-bed reactors, Nuclear Technology.

[22] S. Dong, G. E. Karniadakis, C. Chryssostomidis, A robust and accurate outflow boundary condition for incompressible flow simulations on severely-truncated unbounded domains, Journal of Computational Physics 261 (2014) 83–105.

[23] A. de Klerk, Voidage variation in packed beds at small column to particle diameter ratio, AIChE 49 (8) (2003) 2022–2029.

[24] A. J. Novak, R. W. Carlsen, S. Schunert, P. Balestra, D. Reger, R. N. Slaybaugh, R. C. Martineau, Pronghorn: A multidimensional coarse-mesh application for advanced reactor thermal hydraulics, Nuclear Technology 207 (7) (2021) 1015–1046. arXiv:https://doi.org/10.1080/00295450.2020.1825307, doi:10.1080/00295450.2020.1825307.
URL https://doi.org/10.1080/00295450.2020.1825307

[25] C. J. Permann, D. R. Gaston, D. Andrš, R. W. Carlsen, F. Kong, A. D. Lindsay, J. M. Miller, J. W. Peterson, A. E. Slaughter, R. H. Stogner, R. C. Martineau, Moose: Enabling massively parallel multiphysics simulation, SoftwareX 11 (2020) 100430. doi:https://doi.org/10.1016/j.softx.2020.100430.
URL https://www.sciencedirect.com/science/article/pii/S2352711019302973